# Evaluation of thermal-hydraulics/thermomechanics coupling strategies for the modeling of the behavior of Sodium-cooled Fast Reactors fuel subassemblies under irradiation

F. Acosta, T. Cadiou, V. Blanc, P. Rubiolo

Abstract No: 493 Paper No.:

# Evaluation of thermal-hydraulics/thermomechanics coupling strategies for the modeling of the behavior of Sodium-cooled Fast Reactors fuel subassemblies under irradiation

**Acosta Francisco[1], Cadiou Thierry[1], Blanc Victor[2]**
CEA
*1 - CEA, DEN, DER, SESI, F-13108, Saint Paul lez Durance, France*
*2 - CEA, DEN, DEC, SESC, F-13108, Saint Paul lez Durance, France*
*francisco.acosta@cea.fr*

**Rubiolo Pablo**
*LPSC, University of Grenoble-Alpes, CNRS/IN2P3, F-38026, Grenoble, France*

## ABSTRACT

The fuel pin bundles of Sodium-cooled Fast Reactors (SFR) undergo significant geometrical changes during their irradiation, which affect the coolant flow and temperature distributions in the fuel subassembly, the knowledge of which is necessary for safety assessments. Moreover, as the phenomena responsible for the deformation of the fuel bundles, namely the swelling and creep of the cladding, strongly depend on the temperature, a coupling between the thermal-hydraulic and thermomechanical evolutions of the fuel subassemblies exists. The aim of this paper is to define a methodology for the evaluation of the SFR fuel bundles behavior under irradiation that takes this coupling into account.

To this end, a new numerical coupling has been developed between the industrial Computational Fluid Dynamics (CFD) code Star-CCM+ and a finite element code dedicated to the modeling of the thermomechanical behavior of SFR fuel subassemblies during irradiation, DOMAJEUR2. The coupling is implemented via the exchange of the cladding diametral deformation, calculated by DOMAJEUR2, and its associated temperature field, obtained with Star-CCM+. The sodium mass flow rate reduction expected in the deformed geometries is also taken into account.

A coupled analysis of a 7-pin SFR bundle is presented in this paper. It is shown that, for a high irradiation dose, the deformation induces a significant sodium temperature increase, leading to a cladding maximal surface temperature up to 57°C higher than in a non-deformed bundle. Additionally, the coupled simulations resulted in a diametral strain of the fuel claddings significantly lower (up to -30% locally) than the traditional non-coupled simulations.

## KEYWORDS

COUPLING, CFD, THERMOMECHANICS, THERMAL-HYDRAULICS, SFR

## 1. INTRODUCTION

During their irradiation, Sodium-cooled Fast Reactors (SFR) fuel bundles undergo significant geometric deformation [1], which manifests mainly as diametral strain of the fuel pins claddings, their helical flexion and their ovalisation [2]. These geometrical distortions of the fuel bundle affect the coolant flow and temperature distributions [3-4]. Moreover, since the phenomena that cause the deformation, mainly the swelling and creep of the cladding, are strongly dependent on temperature [5-6], the evolution of the geometry of the fuel bundles and the evolution of their temperature distribution during the irradiation are strongly coupled.

Even though the knowledge of the temperature distribution within the bundle is necessary for safety assessments, the coupling between thermal-hydraulics (TH) and thermomechanics (TM) is still often neglected during the design studies of innovative SFR fuel subassemblies. In fact, a common practice is to disregard the impact of deformation on temperature, and to use the temperature distribution in the non-deformed bundle as input for the TM simulations performed during the design process of the fuel subassemblies.

In recent years, efforts have been made to take this coupling into account. Notably, the work presented in [7], where a sub-channel code has been coupled with a bundle TM code. Besides the sub-channel approach, other more sophisticated Computational Fluid Dynamics (CFD) techniques, such as a Reynolds Averaged Navier-Stokes (RANS) approach, are widely used for nuclear reactor TH calculations. Even though they are normally more time consuming, the latter provide a much higher detail on the flow velocity, pressure, and temperature distributions, and have also been shown to lead to more consistent results than the sub-channel analysis in highly deformed SFR fuel bundles [8].

For these reasons, the present work evaluates a coupling methodology between the industrial CFD code Star-CCM+ V12.02 [9] and a bundle TM analysis code developed at the CEA, DOMAJEUR2, for the modeling of the behavior of SFR fuel subassemblies under irradiation. The goal of this paper is to outline this methodology, and to provide a preliminary estimation of the impact of the coupling between TH and TM for a SFR fuel bundle.

To this end, the TH and TM simulation models and the codes employed are firstly described in section 2, where the coupling methodology and its implementation are also discussed. The irradiation of fictive 7-pin fuel bundle is selected as study case, and the results of its simulation, with and without coupling, are presented in section 3. Finally, the conclusions and perspectives of this work are summarized in section 4.

## 2. THERMAL-HYDRAULIC AND THERMOMECHANICAL SIMULATION OF SFR SUBASSEMBLIES

The objects of the numerical simulations discussed here are the SFR subassemblies, typically containing a bundle of wire-wrapped fuel pins enclosed by a hexagonal can. Their TH and TM modelisations, and the computer codes here employed, are discussed below.

### 2.1. Thermomechanical Simulation

In the context of the R&D efforts for the GEN IV SFR prototype ASTRID [10], DOMAJEUR2, which is a code for the 3D simulation of the TM behavior of SFR subassemblies, is under development at the CEA. It is based on the in-house finite element analysis code Cast3M [11] and it allows considering the thermal, mechanical, and irradiation loads on the subassembly during its lifetime in the reactor, to calculate the evolution of its strain and stress states. The thermal and irradiation creep of the structural materials, as well as their void swelling, are calculated from their temperature, irradiation dose and mechanical stress distributions by means of experimentally determined material laws.

Within DOMAJEUR2, several models with different levels of simplification are available. The most complex one, the *detailed* model, relies on a 3D, volumetric finite element representation of the fuel pin claddings and the hexagonal wrapper can, whereas the spacer wires can be either represented by volumetric finite elements or by 1D beam elements. The thousands of potential contact points between fuel pins in a typical SFR fuel bundle, and the current limitations on computational power, restrict the practical use of this modelisation to subassemblies with up to approximately 19 fuel pins.

A simplified approach, referred to as *project* model, is also available, and it can be employed for the simulation of full scale fuel subassemblies, comprising up to a few hundred fuel pins. In the *project* model, the fuel pins are represented by special 1D hollow beam finite elements, which allow

considering an internal pressure. The model takes into account the thermomechanical and irradiation loads on the cladding to estimate its diametral strain. By representing the fuel pins with a series of 1D beam finite elements, their helical flexion can also be reproduced. Shell-type elements are used for the wrapper hexagonal can. In addition, all potential contact points between elements are linked by transversal, bar-type finite elements that include a model to estimate the stress and strain state of the internal wall of the cladding under the contact point [12][13]. It must be noted that, in the *project* model, the use of 1D beam elements to represent the fuel pins does not allow taking into account the azimuthal temperature gradients present in the circumference of the cladding. This limitation does not exist in the *detailed* model, where the cladding is divided into six azimuthal regions and a different temperature profile is assigned to each of them.

In a simulation using DOMAJEUR2, the irradiation period under consideration is firstly divided into multiple time steps specified by the user. Within each step, the strains and stresses are calculated by means of a nonlinear finite element analysis in the nodes of the model, from which the stresses are then obtained in the integration points of the finite elements. The boundary conditions, such as the time evolution of the cladding temperature distribution, the irradiation dose, and the cladding internal and external pressure, are loaded from a series of input files at the beginning of the simulation.

## 2.2. Thermal-hydraulic Simulation

For the TH simulations of the subassembly, the industrial CFD code Star-CCM+ was selected, both because it has been extensively used for wire-wrapped fuel pin bundle simulations [14-17], and because of its versatile and robust meshing tool that made possible the automatization of the numerous simulations needed for the coupling with a TM code. A RANS approach is employed, and the *all y+* realizable k-ε model is used for the turbulent closure equations. The sodium flow is modeled as incompressible and its thermophysical properties are considered constant and are calculated from the average sodium temperature [18]. Further detail on the modelisation can be found in [3], where it is employed to study ASTRID's fuel bundle.

The simulation domain is circumscribed to the coolant within the heated column of the fuel bundle. That is to say, the sodium surrounding the wire-wrapped fuel pins and enclosed by the hexagonal can, which external and internal surfaces, respectively, are part of the boundaries of the domain; this is schematically represented in Fig. 1 for a 7-pin fuel bundle, where the pin numbering system adopted in this work is also indicated.

The coolant mass flow rate is imposed at the entrance of the domain, where a uniform sodium velocity profile is considered. This approximation was evaluated in a CFD simulation of ASTRID's fuel bundle, where a developed velocity profile was also essayed. The maximum local temperature difference observed between the simulations using a flat and a developed inlet velocity profile was 2°C, the first yielding a higher temperature. The pressure drop within the bundle was not affected by the inlet profile.

A 20 cm long mesh extrusion is added at the exit of the heated column, which allows setting a constant pressure boundary condition downstream the region of interest and improves the convergence rate of the simulations. No-slip boundary conditions are used for all solid walls. The hexagonal can is considered to be adiabatic, as well as the surface of the spacer wires. The heat source is provided by an axial profile of heat flux per fuel pin, which is considered uniform in the circumference of the cladding.

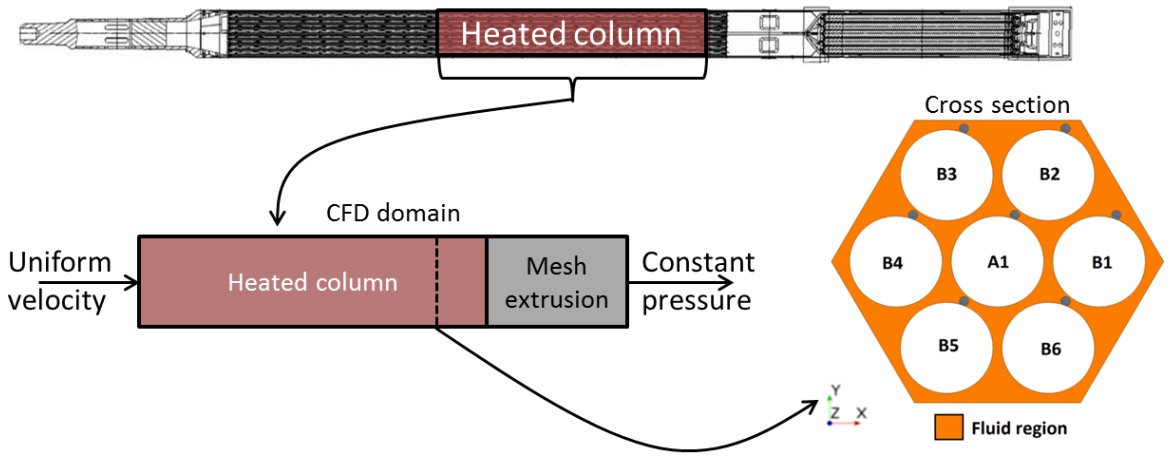


**Fig. 1 Representation of the CFD simulation domain. The fuel pin numbering system is indicated.**

## 2.3. Coupling Methodology

For a simulation with DOMAJEUR2, the temperature histories of the different components of the subassembly - that is, their spatial and temporal temperature distributions during the irradiation – have to be specified. Traditionally, the temperature distribution corresponding to the non-deformed fuel bundle would be used for the whole irradiation period under consideration. In reality, as the irradiation proceeds, the bundle deformation affects the temperature distribution, inducing a gradual overall increase. This temperature increase, in turn, has a feedback effect on the deformation that is caused by the swelling and creep of the materials, which are temperature dependent phenomena.

A rigorous approach to take this coupling into account in a numerical simulation would imply recalculating the temperature field in the deformed geometry obtained at each time step of the TM calculation, and, then, using this field to calculate the strains in the next time step. Nevertheless, DOMAJEUR2 does not yet have the capability of updating, between successive time steps, the temperature history that is loaded at the beginning of the simulation. In addition, performing one CFD calculation per time step can lead to prohibitively high computational costs, not justified if the deformation within the time step is not high enough to induce a perturbation on the temperature field, which is indeed the case until the swelling incubation dose is exceeded. For these reasons, a simplified approach has been adopted in this work, aimed to studying the coupling methodology and to obtaining a first coarse estimation of the impact of the coupling on the behavior of the bundle.

This approach divides the coupled simulation in one initialization stage and one iterative stage. In the first one, a CFD calculation is carried over in the non-deformed geometry, and the temperature distribution thus obtained is used as input for a first TM simulation of the irradiation period under consideration, done with DOMAJEUR2. This first stage, schematically illustrated in Fig. 2 for a given material point within the fuel bundle, corresponds to the traditional practice for the subassembly simulations, and provides here a first estimation of its strain and stress states at the end of the irradiation.

The second stage, schematically presented in Fig. 3 for a given material point within the fuel bundle, starts with the deformed geometry previously obtained. A CFD simulation is carried over in this deformed geometry, and the resulting temperature field, perturbed by the deformation of the bundle, is employed to construct a new temperature history that is used next as input for a new TM simulation. In this history, the temperature distribution obtained in the non-deformed geometry is assigned to the first Full Power Day (FPD) of the irradiation, and the one obtained in the deformed geometry is assigned to the end of the irradiation; DOMAJEUR2 then linearly interpolates the temperature between those times. Evidently, the modified temperature history used for the new TM calculation might lead to a

different deformation level, so this stage is repeated iteratively until two successive iterations yield the same deformed geometry, within a desired tolerance.

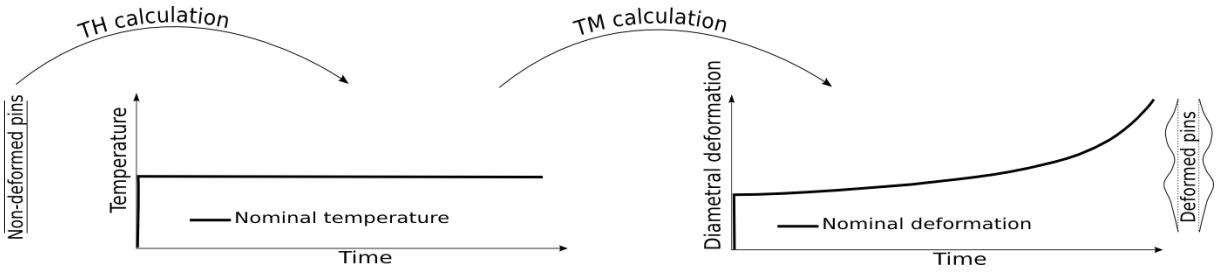


**Fig. 2 Schematic representation of the initialization stage of the coupled simulation, which corresponds to the traditional practice for simulating SFR fuel subassemblies. The temperature and deformation time evolutions correspond to a given point within the fuel bundle.**

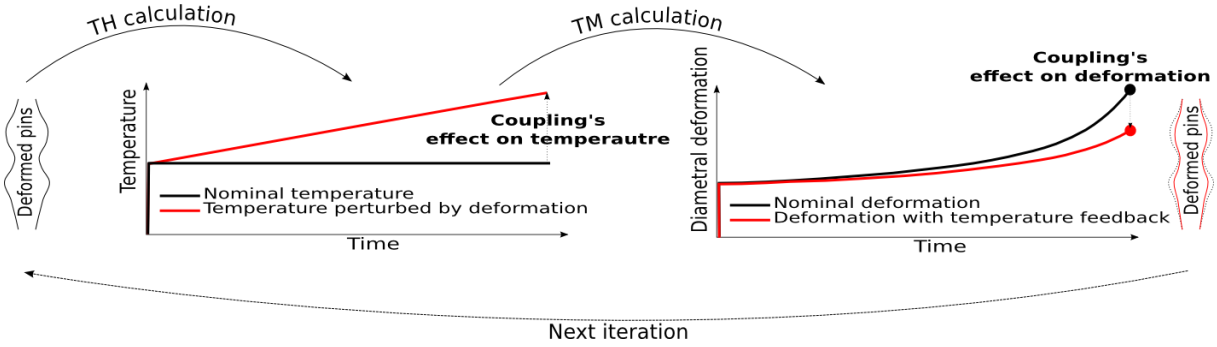


**Fig. 3 Schematic representation of the iterative stage of the coupled simulation. The trends observed for the temperature and deformation distributions in the coupled calculations are represented in red, and correspond to a given point within the fuel bundle.**

## 2.4. Implementation of the Coupling

To implement the procedure outlined in the previous section, an ad hoc numerical platform has been developed. Otherwise user intensive tasks such as the preparation of the DOMAJEUR2 and CFD simulations, as well as their execution and post-processing, have been automated in this platform. This includes the prescription of boundary conditions for the TM calculations that are dependent of the results of the CFD simulations, and vice versa.

### 2.4.1. Generation of the CAD model of the deformed bundle and meshing

Within this platform, the TM simulations are post-treated, and the axial profiles of the radius of the deformed fuel pins, within their heated column, are employed to construct a 3D CAD representation of the deformed bundle, which is required for the CFD simulations. To generate this geometry, the radius profile of each pin is rotated about its axis- that corresponds to the pin's centreline- and then the spacer wire is wrapped around the rotational body's surface. An interference of 5% of the wire's diameter is introduced between the wire and the cladding in order to avoid the line contact which is very difficult to mesh. This simplification has been shown to be a reasonable compromise to model the spacer wire [17]. The wire's swelling is neglected.

In the CAD representation, the positions of the axis of all pins are not modified from the nominal geometry. So, depending on the deformation level, there might be contact between the pins and the neighbouring wires, and the spacer wires are allowed to penetrate into neighbouring pins. This is, of course, not the case in a real bundle, were additional diametral strain is accommodated by other deformation mechanisms, such us cladding ovalisation or helical flexion. This simplification leads to a

higher cross section available for the sodium flow. However, in the most deformed bundle evaluated in this work, the interference between pins and neighbouring wires led to an increment of only 0.6% of the average cross section available for sodium flow, with respect to a geometry with the same deformation but without wire-cladding interpenetration. The average cross section reduction associated to the deformation is 35 times higher than the increment caused by the interpenetration, which likely makes the latter effect of second order.

Even though the fuel pins present other deformation mechanisms, such as helical bowing and ovalisation (calculated by DOMAJEUR2), they are not taken into consideration in this first approach, since only the diametral strain affects the hydraulic diameter of the bundle at a given axial position, which, in turn, impacts the mass flow rate imposed as boundary condition for the CFD simulations. Finally, the hexagonal can is not modified from its nominal geometry to construct the CAD representation. This approximation is in agreement with available experimental data on the hexagonal can of the highly irradiated PHENIX's BOITIX9 fuel subassembly, which presented excellent dimensional stability during irradiation with only up to 0.5% volume swelling [10].

After the construction of the CAD model of the deformed bundle, a volume mesh is generated using Star-CCM+'s automated meshing tool, which, based on global parameters such as a target cell size, allows creating a good quality mesh using, in this case, polyhedral cells in the core of the fluid volume and one layer of prismatic cells on the solid boundaries of the domain. This technique has been shown to provide good results both in non-deformed and deformed SFR bundles geometries [3-4].

### 2.4.2. Deformation dependent boundary conditions for the CFD simulation

Next, the boundary conditions have to be specified. Among these, the wall heat flux profile of the fuel pins and the mass flow rate at the inlet of the bundle depend on the level of deformation. Consequently, the heat flux is recalculated keeping the linear power profile of the pins constant, which implies that the potential neutronic feedback is neglected. In addition, a model to estimate the mass flow rate in the deformed geometry has been implemented so that it can be automatically adjusted.

The mass flow rate estimation model is based on fuel bundle pressure drop correlations and on preexisting CFD simulations, and it is detailed in [3]. Even though only the heated length of the fuel bundle is considered in the CFD simulations, the relationship between mass flow rate and deformation depends also on the geometry of the rest of the fuel subassembly, including its foot and upper section. For the model here implemented, one ASTRID fuel subassembly is considered to undergo significant geometrical deformation within a non-deformed core. This situation can understood as an idealized representation of the experimental irradiation of one subassembly, which typically remains in the core for a longer period of time than the rest of the subassemblies and, as a consequence, undergoes a much higher deformation. In this case, the increased hydraulic resistance of the deformed bundle would divert some of the coolant flow towards the neighboring, less-deformed fuel subassemblies. The main simplifying hypotheses of the model are:

- Only the diametral strain of the heated length of the fuel pins is considered.
- All the fuel assemblies present the same pressure drop between their inlet and outlet, and it is the same as the core's pressure drop $\Delta P_{core}$. This assumption is based on the existence of lower and upper plena that communicate, respectively, the inlets and outlets of all fuel assemblies. Current CEA experience indicates that the radial pressure gradients in these plena are minor.
- The variation of $\Delta P_{core}$ with the deformation of only one of its more than 200 fuel assemblies is neglected.

### 2.4.3. Generation of the cladding temperature history and DOMAJEUR2 simulation

Finally, after the boundary conditions are set, the CFD calculation is run and post-treated to obtain the

temperature distribution in the fuel pins external surface. The cladding surface temperature, and the local linear power and diameter of the deformed pin, are used to compute the temperature in the mid-thickness of the cladding, by means of a 1D radial heat conduction model. The resulting cladding temperature distribution is employed to construct, as described in section 2.3, the temperature history required for the DOMAJEUR2 calculation, which is then performed.

## 3. ANALYSIS OF A SIMPLIFIED STUDY CASE

In order to evaluate the impact of the coupling between TM and TH on the evolution of SFR fuel bundles under irradiation, and to analyze different modelisation options, a bundle of 7 wire-wrapped fuel pins enclosed in an hexagonal can was selected as study case. The number of pins was kept low so that the *detailed* model of DOMAJEUR2 could be employed. The geometrical parameters and the TH boundary conditions were chosen to be representative of ASTRID reactor, and are presented in Table 1. Two different irradiation dose profiles, with a maximum of 123 displacements per atom (dpa) and 165 dpa respectively, were evaluated, and they are presented in Fig. 4 together with the linear power profile used in all simulations. There and in the rest of this paper, the axial positon is measured from the lower end of the heated column of the bundle. For comparison, a record dose of 160 dpa has already been reached in the BOITIX9 fuel bundle in PHENIX SFR [19]. The central region with lower power and irradiation dose observed in Fig. 4 is characteristic of the axially heterogeneous fuel pin design of ASTRID reactor, in which a central fertile column is included.

**Table 1. Geometrical and thermal-hydraulic characteristics of the 7-pin fuel bundle.**

| Parameter | Value |
|---|---|
| Heated column length | 0.8 m |
| Fuel pin pitch | 10.8 mm |
| Fuel pin external diameter | 9.7 mm |
| Spacer wire diameter | 1.0 mm |
| Spacer wire helix step | 180 mm |
| Maximum linear power | 550 W/cm |
| Mass flow rate in nominal conditions | 1.2 kg/s |
| Inlet sodium temperature | 400 °C |

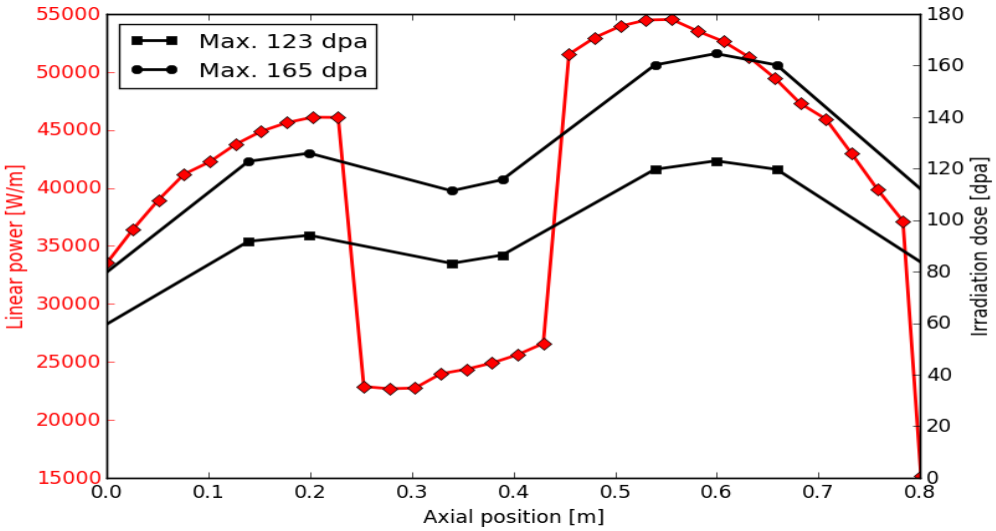


**Fig. 4 Axial profiles of linear power and irradiation dose employed for the numerical simulations.**

A homogeneous diametral strain of the heated column of ASTRID fuel bundle has been shown to induce very significant sodium temperature increases, with respect to a non-deformed bundle [3]. In

this work, we firstly study the effects on TH of a more realistic representation of the pins deformation, where the strain profile is obtained with a TM simulation of the bundle's irradiation. To do so, CFD simulations were carried over in the non-deformed, nominal geometry, and were compared with the ones conducted in two deformed geometries obtained with DOMAJEUR2 by using different irradiation dose levels. The first one presents an average diametral deformation of 2.0 %, corresponding to an End Of Life (EOL) maximum irradiation dose of 123 dpa, while the average diametral strain of the second one is 4.9 %, associated to a maximum dose of 165 dpa. It is worth noting that, even though the same irradiation dose profile was employed for all fuel pins, they present different deformation levels due to the non-uniform temperature distribution within the bundle.

The procedure outlined in 2.4.1 was employed to generate the mesh for the CFD simulations in the three cases analyzed. This resulted in a cell count of between 2.0 and 2.3 million, depending on the deformation level. The *all y+* treatment adopted provides more accurate results when the non-dimensional wall distance, y+, lies outside the buffer layer ( that is, 5<y+<30 approximately), even though a blending approach between high y+ and low y+ treatment creates reasonable solutions in these intermediate cells. In the simulations here evaluated, less than 20% of the near wall cells present wall y+ values between 5 and 30, and they are concentrated around the contact lines between the fuel pins and their spacer wires. For this preliminary study, this was judged to be adequate. Constant sodium properties for a temperature of 475°C (average between inlet and outlet of the bundle in nominal conditions) were employed.

As discussed in 2.4.2, the mass flow rate imposed at the inlet of the CFD domain depends not only on the bundle's deformation, known here, but also on the characteristics of the rest of the fuel subassembly, such us the hydraulic resistance of the subassembly foot. The fictive 7-pin bundle here analyzed does not have a counterpart in reality. For this reason, and to be representative of ASTRID's behavior, the mass flow rate percentage reduction was considered to be equal to that of ASTRID for the same bundle deformation level, so the model outlined in 2.3.2 was employed. This resulted in a 6% mass flow rate reduction for the less deformed bundle, while a 17% reduction was obtained for the more deformed one.

### 3.1. Effects of Deformation on Thermal-hydraulics

The axial profile of sodium bulk temperature is presented, for the three deformation levels, in Fig. 5, together with the cladding surface temperature profiles for the central pin of each bundle. Increases of average sodium temperature of 9°C and 30°C are observed at the outlet of the heated column of the less and more deformed geometries, respectively, with respect to the non-deformed bundle. The cladding surface temperature profiles presented were obtained by averaging, for each axial position, the temperature over one sixth of the cladding circumference, and they correspond to the cladding arc centered on the point closest to pin B1, indicated in the diagram by a red cross. It can also be observed that the local perturbations due to the spacer wires are augmented as the deformation increases.

In addition, the maximum cladding surface temperature, obtained by averaging over on sixth of the claddings circumferences, increases from 600°C in the nominal geometry to 657°C in the most deformed bundle, and the dispersion in the maximum temperature of the different fuel pins is also augmented with the deformation. Its standard deviation increases from 4.7°C in the nominal geometry to 8.1°C in the most deformed one.

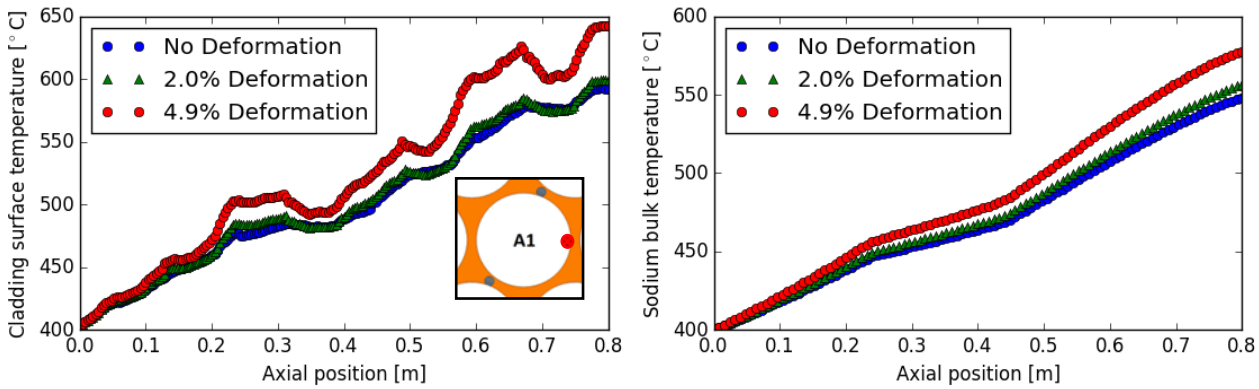


**Fig. 5 Cladding surface temperature along the heated length of the central pin for the line closest to pin B1 (left) and axial profile of sodium bulk temperature (right) for the deformed and non-deformed bundles.**

Furthermore, the azimuthal temperature gradients around the fuel pins are greatly increased by the deformation. To illustrate this, the peripheral pin B6 was selected. The sodium temperature on its surface was sampled every 60 degrees, at the outlet of the heated column of the bundle, and its distribution around the pin's circumference is presented in Fig. 6 for the 3 deformation levels evaluated. The increase of the azimuthal temperature gradients with deformation is evidenced by the departure from the regular hexagon shape that would be obtained in a zero gradient case. The maximum temperature difference between diametrically opposed points on the cladding's surface increases with deformation. In particular, the difference between the maximum and minimum temperature computed at those 6 points increases from 62°C in the nominal geometry to 66°C in the 2.0% deformed geometry and to 96°C in the 4.9% deformed geometry.

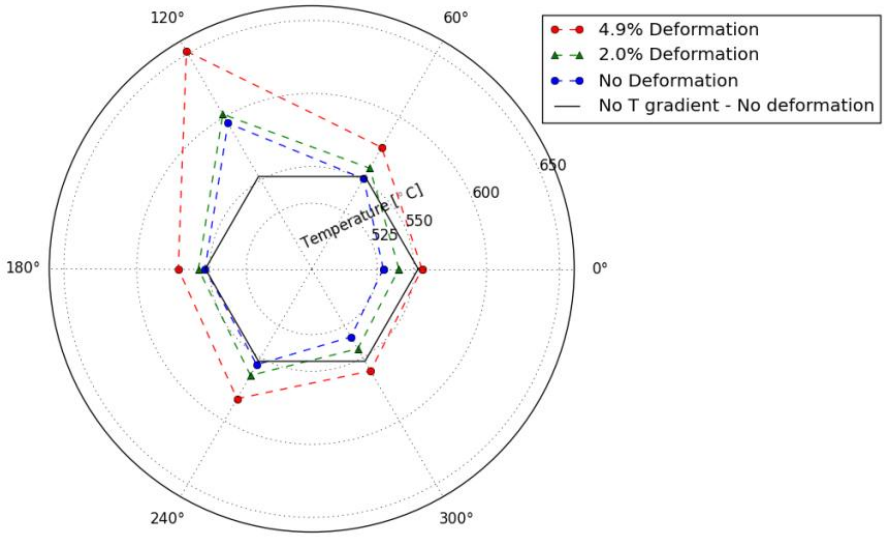


**Fig. 6 Temperature distribution around the peripheral pin B6, at the outlet of the heated column, in the deformed and non-deformed geometries.**

Additionally, the deformation of the bundle leads to the contact between spacer wires and neighboring fuel pins, which, besides potentially leading to hot spots in the cladding next to the point of contact, induce local sodium flow disruptions. As an example, Fig. 7 illustrates how the contact between spacer wires and neighboring pins, at the outlet of the heated column, completely blocks the sodium flowing from the colder periphery to the hotter central region, and vice versa, in the regions where contact

occurs.

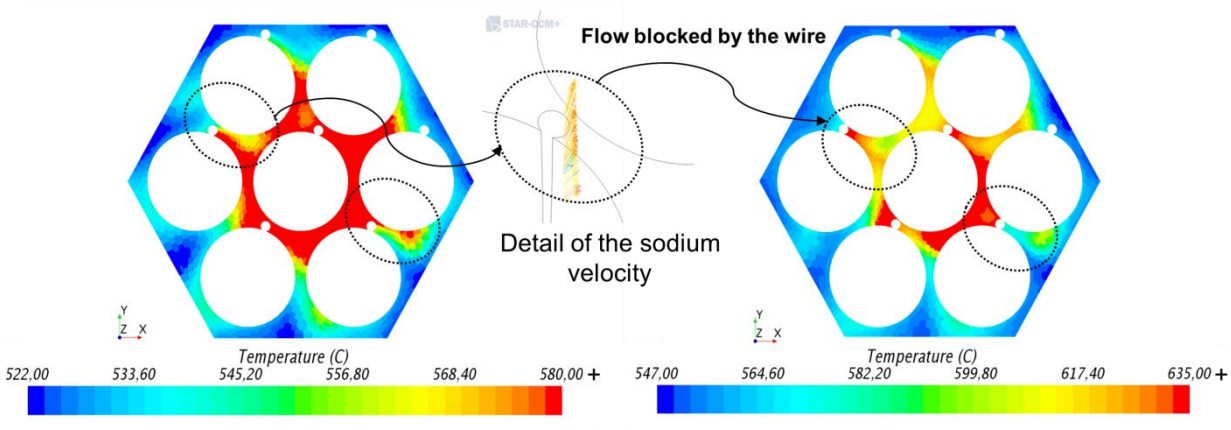


**Fig. 7 Sodium temperature at the outlet of the heated column of the non-deformed (left) and deformed (right) bundle. The sodium velocity vectors in one of the gaps closed by the deformation is also presented (center).**

The temperature perturbation described above, induced by the deformation, has a feedback on thermomechanics. To assess this effect, coupled TM/TH simulations of the 7-pin study case were conducted, and the results are presented hereafter.

## 3.2. Effects of the Coupling on the Bundle Deformation

The irradiation of the 7-pin bundle was simulated employing the coupling methodology described in 2.3 for the two different dose levels presented in Fig.4 and evaluated in 3.1. The *detailed* model of DOMAJEUR2 was adopted.

For the lower dose profile with a maximum of 123 dpa, the temperature increase evidenced in 3.1 was not high enough to provide a significant feedback on the deformation of the bundle. Therefore, in this case, the deformed geometry obtained with the coupled simulation does not significantly differ from the one obtained in the non-coupled calculation using the nominal temperature distribution.

For the higher dose profile with a maximum of 165 dpa, on the other hand, the deformation level is higher and it induces a greater temperature increase. In this case, the EOL deformation of the bundle obtained with the coupling is significantly lower than the one obtained using only the nominal temperature distribution as input for the TM calculations. This can be observed in Fig. 8, where the average diametral strain profiles of the central and one peripheral pin obtained with and without coupling between TH and TM are presented. It can be there observed that, in the upper half of the heated column, the coupling leads to a diametral strain up to 30% lower than the non-coupled simulation.

The observed effect can be explained by the temperature dependence of the physical phenomena that cause the deformation, mainly swelling and irradiation creep. The cladding swelling estimated by the empirical law employed for the TM simulations is presented in Fig. 9 as a function of temperature, for two different irradiation doses corresponding to the maxima of the dose profiles evaluated in this work. It can be noted that there is one temperature for which swelling is maximized, which increases with the irradiation dose. The irradiation creep presents a similar temperature dependence. Therefore, the observed reduction in deformation is explained by the departure from the temperature range that maximizes swelling and irradiation creep, as can be observed in Fig. 10, where these ranges are plotted – for a dose range of [100,165] dpa - together with the temperature profiles of the central and one peripheral pin in the non-deformed geometry. It can be seen there that, in the upper half of the heated column, the temperature of both pins is superior to that that maximizes swelling and irradiation

creep, thus a temperature increment would lead to a lower deformation level.

The impact of the coupling on the deformation is higher in the upper half of the heated column. This is firstly due the higher temperature perturbation in this region with respect to the nominal temperature distribution, as can be noted in Fig. 5. Additionally, as can be observed in Fig. 10, the cladding temperature in the non-deformed geometry is, in the lower part of the heated column, closer to the temperature level that maximizes swelling and irradiation creep, around which their partial derivatives with respect to temperature have a smaller absolute value (See Fig. 9).

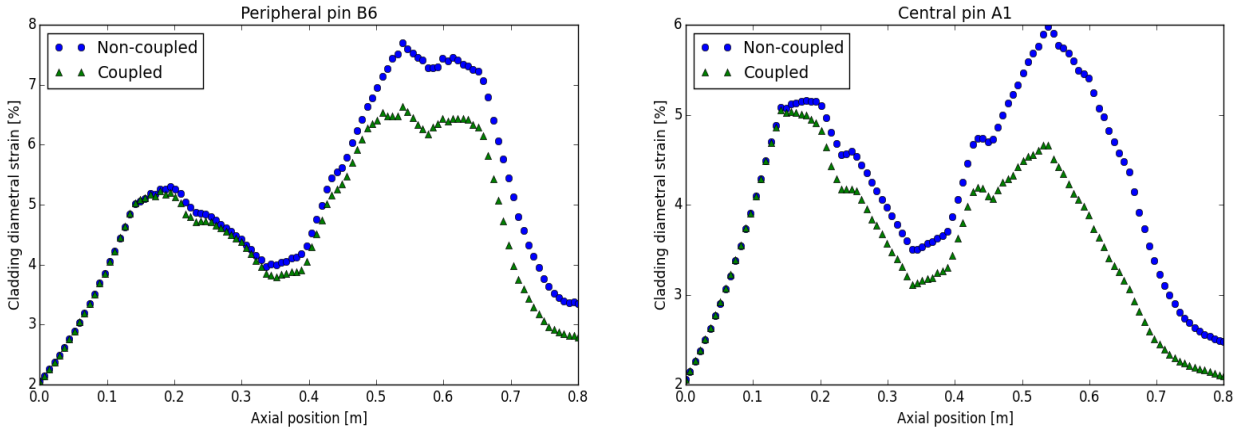


**Fig. 8 Diametral strain of the cladding of the peripheral pin B6 (left) and the central pin (right) along the heated column, obtained with and without TM/TH coupling.**

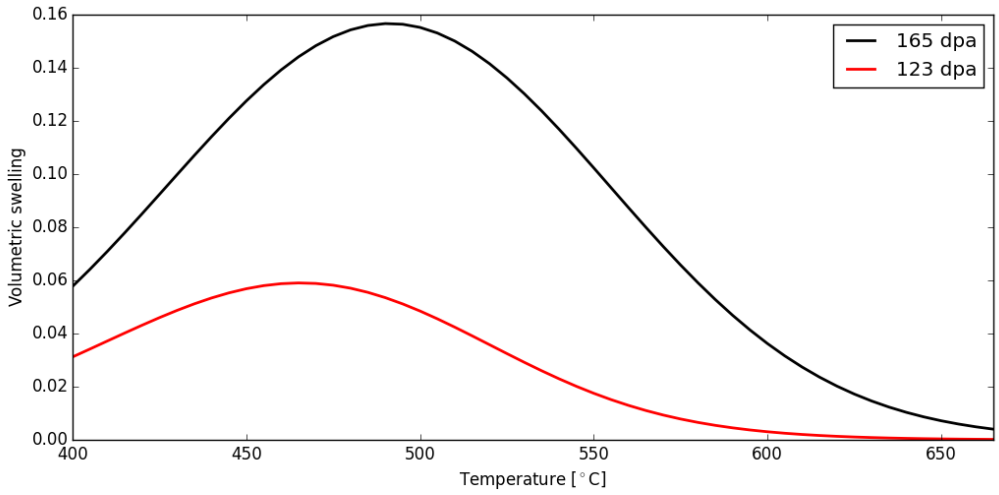


**Fig. 9 Empirical law of the cladding swelling as a function of temperature, for two different irradiation dose levels.**

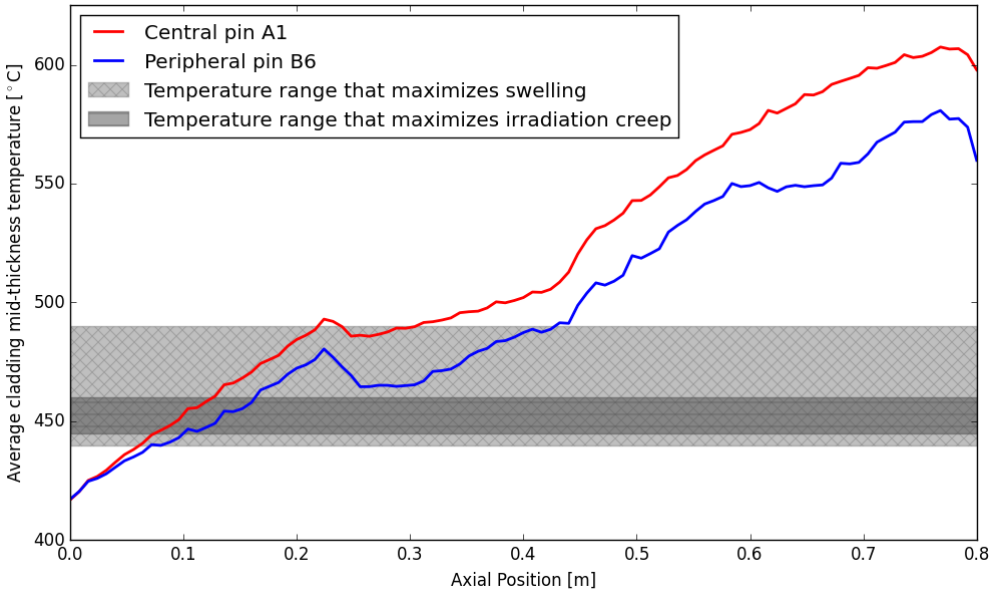


**Fig. 10 Average cladding temperature along the heated column of the central and one peripheral pin of the non-deformed bundle. The temperature ranges that maximize swelling and irradiation creep -for a dose range of [100,165] dpa- are indicated.**

## 3.3. Impact of the Azimuthal Temperature Gradients on the Cladding's Diametral Strain

Even though the temperature gradients around the circumference of the claddings were shown to be high (see Fig 6), their impact on diametral deformation is very limited. This can be observed in Fig. 11, where the diametral deformation profiles of a peripheral pin of the bundle calculated with DOMAJEUR2 using 6 temperature axial profiles around the cladding circumference – one every 60 degrees – is compared to the one obtained using only one averaged profile per pin. For the lower dose essayed, using 6 profiles leads to a diametral strain 1.2 % higher than using only one, and the maximum local difference is 5%. For the higher dose, no significant differences are observed. For both dose levels, the calculations with only one temperature profiles per pin demanded significantly less computation time.

Although the impact of the azimuthal temperature gradients on the stress state of the cladding is yet to be quantified, their low impact on the diametral deformation of the fuel pins, on which the coupling here developed is based, suggests that the *project* model of DOMAJEUR2, that only allows using one temperature profile per fuel pin, might be a reasonable option for the coupling methodology. For this reason, this simplified model is next compared to the *detailed* approach.

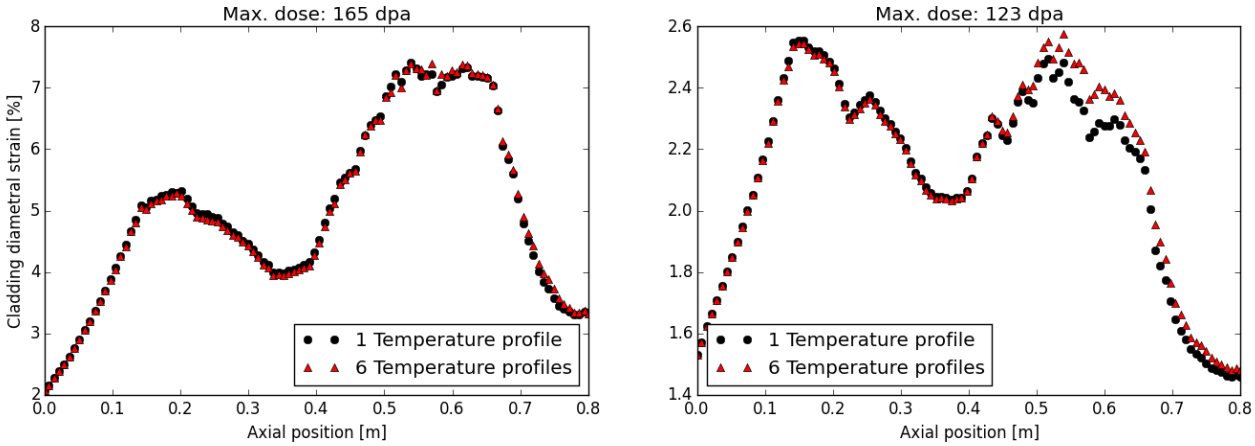


**Fig. 11 Diametral strain profile of the peripheral pin B6 obtained with DOMAJEUR2 using one and six axial temperature profiles per pin, for a maximum dose of 165 dpa (left) and 123 dpa (right).**

### 3.4. *Detailed* vs *Project* Thermomechanical Modelisations

The irradiation of the 7-pin bundle was simulated using the *detailed* and the *project* models of DOMAJEUR2, for two irradiation dose levels. Six cladding temperature profiles were employed per pin in the *detailed* model, while one average profile was used per pin in the *project* simulations.

The axial profiles of cladding diametral strain obtained with each model are presented in Fig. 12 for the central pin, which evidenced the highest differences between models, for the two dose levels evaluated. For 123 dpa, the *detailed* model led to an average diametral strain 1% lower than the *project* one, while it yielded a deformation 7% higher for 165 dpa. The azimuthal temperature gradients in the pins' circumferences, not considered in the *project* modelisation, were shown to have a negligible impact on the diametral strain of the most irradiated bundle (see Fig. 11), so they cannot explain the difference found between the two models. The cladding plastic strain obtained with both models was found to be in good agreement, and ongoing studies suggest that the observed difference might be linked to the elastic strain induced by the helical flexion of the fuel pins, which is underestimated in the *project* simulations.

It can also be noted that the maximum deformation obtained with the two models is in very good agreement and that, for the most irradiated pin, the difference in diametral strain is concentrated in the upper part of the heated column. Since both the deformation level and the linear power are relatively low in this region, the higher strain obtained with the *detailed* model only led to a 10°C increase in the maximum cladding surface temperature - calculated by averaging over one sixth of the cladding's circumference-, over which operational limits are imposed in SFR for safety reasons. This difference is reduced to 5°C if the same mass flow rate is used for both simulations, instead of calculating, as described in 2.4.2, the mass flow rate reduction that corresponds to each deformed bundle. The impact of the strain difference on the average cladding temperature at a given axial position is even smaller, averaging less than 5°C in the upper half of the central pin, were the effect was most noticeable. In addition, both models led to the same maximum volume swelling of the cladding, on which one of the most limiting design criteria of ASTRID subassemblies is based.

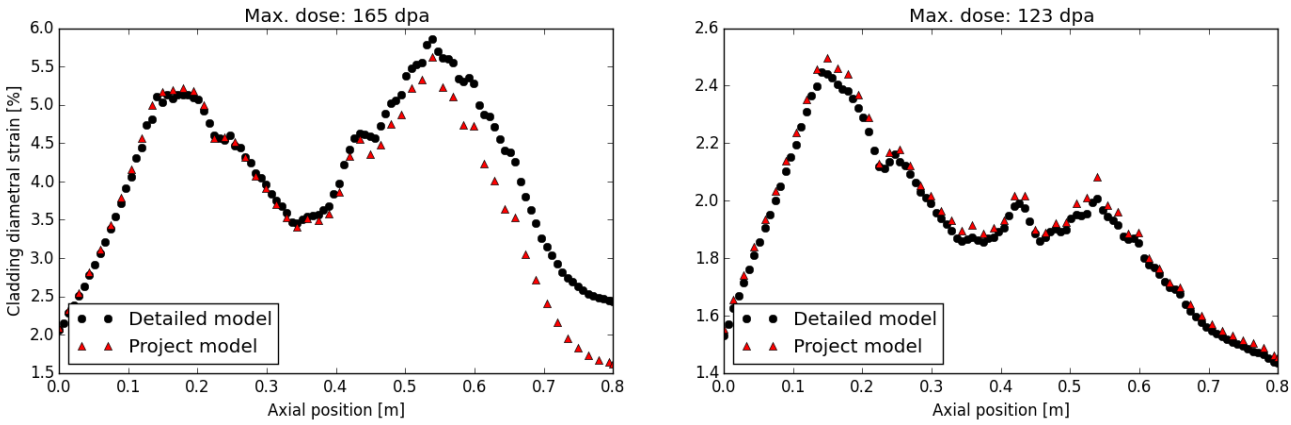


**Fig. 12 Diametral strain profile of the central pin obtained with the *detailed* and *project* models of DOMAJEUR2, for a maximum dose of 165 dpa (left) and 123 dpa (right).**

## 4. CONCLUSIONS AND PERSPECTIVES

A new numerical simulation platform, designed to study the behavior under irradiation of SFR fuel bundles taking into account the TM/TH coupling, which arises from the temperature dependence of swelling and creep, was introduced in this paper. This platform is based on the coupling of a commercial CFD code, Star-CCM+, with a bundle TM code developed at the CEA, DOMAJEUR2, implemented via the exchange of cladding diametral strain and temperature profiles between the two codes.

A 7-pin fuel bundle with geometrical and TH characteristics similar to that of ASTRID reactor was selected to evaluate the effects of the deformation of the bundle, here represented by axially non-uniform cladding diametral strain profiles, on its TH. Then, the effects of the coupling between TH and TM were assessed.

For an irradiation dose close to the highest recorded for an SFR fuel subassembly, the calculated bundle deformation led to an increase of the maximum cladding surface temperature of 57°C, and also increased the average sodium outlet temperature and the azimuthal temperature gradients within the pins' circumferences.

Consequence of the temperature increases caused by the bundle deformation, the coupled calculations for that same dose level led to a significant reduction of the EOL diametral strain of the fuel pins, with respect to a non-coupled calculation. In the most affected parts of the fuel bundle, this reduction reached 30%, and it is explained by the temperature dependence of swelling and irradiation creep.

The comparison between a thermomechanical simulation conducted with several temperature profiles per pin and one with only one average temperature profile per pin showed that the high temperature gradients in the claddings circumferences do not present a significant effect on the diametral strain. For this reason, a simplified TM model that does not take them into account was compared to a more complex- and computationally expensive- one that does. They were found to be in very good agreement on the calculation of the maximum diametral strain and of the volumetric swelling of the cladding, though higher local diametral strain differences were observed in the upper part of the fuel bundle. Since these differences presented a limited impact in the bundle's TH, and considering that the simplified TM approach is the only one that can be practically employed for full-size SFR fuel bundles, it seems to be adequate for the coupling platform under development.

In the near future, the intention of the authors is to further develop the coupled simulation platform by considering, in the CFD simulations, other bundle deformation mechanisms, such is the fuel pins helical bowing. More frequent updates of the temperature field used during the TM calculations, here

replaced by a linear interpolation between BOL and EOL, are also under consideration. Finally, the results obtained with this platform will be contrasted with existing experimental data.

## REFERENCES

1. K. Katsuyama, T. Nagamine, S. Matsumoto, and S. Sato, 'High energy X-ray CT study on the central void formations and the fuel pin deformations of FBR fuel assemblies', *Nuclear Instruments and Methods in Physics Research Section B: Beam Interactions with Materials and Atoms*, **255**(2), pp. 365–372 (2007).
2. J. Guidez, *Phénix : Le retour d'expérience,* pp. 73-74, EDP Sciences, France (2013).
3. T. Cadiou and F. Acosta, 'The impact of the fuel pin bundle deformation on the thermal-hydraulics of ASTRID sub-assembly', *12th International Topical Meeting on Nuclear Reactor Thermal-Hydraulics, Operation and Safety (NUTHOS-12)*, Qingdao, China (2018).
4. E. Sosnovsky, E. Baglietto, S. Keijers, K. V. Tichelen, T. C. de Souza, H. Doolaard, and F. Roelofs, 'CFD simulations to determine the effects of deformations on liquid metal cooled wire wrapped fuel assemblies', *Proceedings of the 16th International Topical Meeting on Nuclear Reactor Thermalhydraulics (NURETH-16)*, Chicago, USA (2015).
5. E. R. Gilbert and J. F. Bates, 'Dependence of irradiation creep on temperature and atom displacements in 20% cold worked type 316 stainless steel', *Journal of Nuclear Materials*, **65**, pp. 204–209 (1977).
6. M. P. Surh, J. B. Sturgeon, and W. G. Wolfer, 'Radiation swelling behavior and its dependence on temperature, dose rate, and dislocation structure evolution', *Journal of Nuclear Materials*, **336**(2), pp. 217–224 (2005).
7. T. Uwaba, H. Ohshima, and M. Ito, 'Analyses of deformation and thermal-hydraulics within a wire-wrapped fuel subassembly in a liquid metal fast reactor by the coupled code system', *Nuclear Engineering and Design*, **317**, pp. 133–145 (2017).
8. E. Baglietto, J.W Fricano, E. Sosnovsky, ' CFD Activities in Support of Thermal-hydraulic Modeling of SFR Fuel Bundles', *Proceddings of the 10th International Topical Meeting on Nuclear Thermal-Hydraulics, Operation and Safety (NUTHOS-10)*, Japan (2014).
9. STAR-CCM + v12.02 Users Manual (2017).
10. T. Beck *et al.*, 'Conceptual design of ASTRID fuel sub-assemblies', *Nuclear Engineering and Design*, **315**, pp. 51–60 (2017).
11. 'Presentation of Cast3M': http://www-cast3m.cea.fr/index.php?xml=presentation (2018).
12. B. Leturcq, JB. Minne, F. Di Paola, 'Nouvel élément de structure pour les calculs d'interaction dans les faisceaux d'aiguilles combustibles des RNR', *13ème Colloque National en Calcul des Structures,*Var, France (2017).
13. B. Leturcq, J.B Minne, F. Di Paola, *'A new structural behavior to perform efficient nonlinear SFR fuel bundle thermomechanical analysis'*, presented at the Club Cast3M 2016, available at http://www-cast3m.cea.fr/index.php?xml=clubcast3m2016 (2016).
14. J. W. Fricano and E. Baglietto, 'A quantitative CFD benchmark for Sodium Fast Reactor fuel assembly modeling', *Annals of Nuclear Energy*, **64**, pp. 32–42 (2014).
15. E. Merzari *et al.*, 'Benchmark exercise for fluid flow simulations in a liquid metal fast reactor fuel assembly', *Nucl Eng Des*, **298**, pp. 218–228 (2016).
16. T. Cadiou and A. Saxena, 'Thermal–hydraulic numerical simulation of fuel sub-assembly using a dedicated meshing tool', *Nuclear Engineering and Design*, **295**, pp. 162–172 (2015).

17. U. Bieder, V. Barthel, F. Ducros, P. Quéméré and S. Vandroux, 'CFD calculations of wire wrapped fuel bundles: modeling and validation strategies', *Workshop Proceedings of Computational Fluid Dynamics for Nuclear Reactor Safety Applications (CFD4NRS-3),* Bethesda, USA (2010).
18. P. Petiot and J.M Seiler, 'Physical properties of sodium : a contribution to the estimation of critical coordinates', *High Temperatures - High Pressures*, **16**(3), pp. 289-293(1984).
19. J.L Seran *et al,* 'Behavior under Neutron Irradiation of the 15-15Ti and EM10 Steels Used as Standard Materials of the Phénix Fuel Subassembly', *Proceedings of the 15th International Conference on Effects of Radiation on Materials*, ASTM-STP, **1125**, (1992)